FULL PAPER

Gas-Phase Models for the Nickel- and Palladium-Catalyzed Deoxygenation of Fatty Acids

Kevin Parker,[a] Dr. Geethika K. Weragoda,[b] Victoria Pho,[a] Prof. Allan J. Canty,[c] Prof. Anastasios Polyzos,[b,d] Prof. Richard A. J. O'Hair,*[e] Prof. Victor Ryzhov,*[a]

[a] K. Parker, V. Pho, V. Ryzhov
@kevinparker_138
Department of Chemistry and Biochemistry
Northern Illinois University
DeKalb, IL 60115, USA
E-mail: ryzhov@niu.edu
[b] G.K. Weragoda, A. Polyzos
CSIRO Manufacturing
Research Way, Clayton VIC 3168, Australia
[c] A.J. Canty
School of Natural Sciences-Chemistry
University of Tasmania
Private Bag 75, Hobart, Tasmania 7001, Australia
[d] A. Polyzos
School of Chemistry
The University of Melbourne
Victoria 3010, Australia
[e] R.A.J. O'Hair
School of Chemistry
Bio21 Institute of Molecular Science and Biotechnology
The University of Melbourne
Victoria 3010, Australia
E-mail: rohair@unimelb.edu.au

Supporting information for this article is given via a link at the end of the document

Abstract: Using fatty acids as renewable sources of biofuels requires deoxygenation. While a number of promising catalysts have been developed to achieve this, their operating mechanisms are poorly understood. Here, model molecular systems are studied in the gas phase using mass spectrometry experiments and DFT calculations. The coordinated metal complexes $[(phen)M(O_2CR)]^+$ (where phen = 1,10-phenanthroline; M = Ni or Pd; R = C_nH_{2n+1}, n≥2) are formed via electrospray ionization. Their collision-induced dissociation (CID) initiates deoxygenation via loss of CO_2 and $[C,H_2,O_2]$. The CID spectrum of the stearate complexes (R = $C_{17}H_{35}$) also shows a series of cations $[(phen)M(R')]^+$ (where R' < C_{17}) separated by 14 Da (CH_2) corresponding to losses of C_2H_4-$C_{16}H_{32}$ (cracking products). Sequential CID of $[(phen)M(R')]^+$ ultimately leads to $[(phen)M(H)]^+$ and $[(phen)M(CH_3)]^+$, both of which react with volatile carboxylic acids, RCO_2H, (acetic, propionic, and butyric) to reform the coordinated carboxylate complexes $[(phen)M(O_2CR)]^+$. In contrast, cracking products with longer carbon chains, $[(phen)M(R)]^+$ (R > C_2), were unreactive towards these carboxylic acids. DFT calculations are consistent with these results and reveal that the approach of the carboxylic acid to the "free" coordination site is blocked by agostic interactions for R > CH_3.

Introduction

Production of petroleum-diesel-like hydrocarbons from animal and vegetable fats is a renewable and cleaner energy source than traditional fossil fuels[1]. Biomass is already being used for fuel and energy production in many places and has become of great interest to fuel companies with many applications[1–4]. These include the various methods for paraffinic fuel production where there has been recent progress[5,6]. Another common method for production of biodiesel from vegetable and animal fats is by transesterification with methanol that has many industrial-scale applications[7]. While this is a well-established method for production of renewable liquid fuels, the poor storage stability and marginal cold flow properties can outweigh the good cetane number and lubricity of these fuels. Thus, there is an ongoing effort to develop drop-in replacements for petroleum-derived fuels from fatty acids and triglycerides that would possess more desirable properties. Some of these methods rely on toxic chemicals and high pressures of hydrogen gas[8]. Finding a new way to produce hydrocarbons which can be used as fuel and organic starting materials would significantly reduce their need from non-renewable resources.

One of the most promising methods for the conversion of biomass to hydrocarbons is through deoxygenation of fatty acids [7,9,10]. In the absence of a metal catalyst, pyrolysis of fatty acids proceeds via competing decarboxylation and dehydration pathways[11]. Pioneering work by Sabatier has shown that deoxygenation of carboxylic acids proceeds via either decarboxylation, dehydration with decarbonylation, or a combination of both [12], illustrated by Eqns. 1 and 2 for stearic acid. In the absence of a metal catalyst, carboxylic acids favored the decarboxylation route, however, with the addition of an appropriate metal catalyst, any of the three pathways can be

favored [12]. Through deoxygenation and cracking, fatty acids can be turned into smaller linear hydrocarbons of varying length. Oxygen removal through decarboxylation or a combination of dehydration and decarbonylation are all catalyzed by various metals, with more recent studies showing platinum, palladium, and nickel as highly efficient catalysts[13,14]. In addition, tungsten(VI) and molybdenum(VI) oxides have been used.[14,15] Cracking reactions can occur at high temperatures with fatty acids alone, however the addition of metal catalysts can lower the energy needs and increase product formation at lower temperatures, thus reducing energy requirements.[7,12]

$$C_{17}H_{35}CO_2H \rightarrow CO_2 + \text{alkane} \quad (1)$$

$$C_{17}H_{35}CO_2H \rightarrow CO + H_2O + \text{alkene} \quad (2)$$

Metal-catalyzed deoxygenation of stearic acid has been previously described to be dominated by decarboxylation and decarbonylation/dehydration. Decarboxylation is thermodynamically favored, however, with the right metal catalyst, decarbonylation can also be observed[16]. Recently a dual metal photocatalysis approach for the selective conversion of fatty acids into to alpha-olefins (Eq. 3) has been described[17]

$$C_{17}H_{35}CO_2H \rightarrow CO_2 + H_2 + C_{15}H_{31}CH{=}CH_2 \quad (3)$$

Gas-phase ion chemistry has been used to study metal-induced decomposition of fatty acids for several decades. Schröder et al. showed that Fe^+ ions can mediate dehydrogenation and decarbonylation of fatty acids[18]. Similarly, Yalcin and co-workers showed that Ni^+ can cause dehydrogenation and dehydration paired with decarbonylation of aliphatic amino acids, as well as alkene losses[19]. More recently, the focus has shifted to metal catalysts in their natural oxidation states. For example, ternary complexes of the general formula $[(L)M(O_2CR)]^+$ where M = Co, Ni, and Zn and L =2,2'-bipyridyl can be easily observed in ESI MS[20]. Corresponding Cu^{2+} complexes lose the whole carboxylate radical upon collisional activation, forming a reduced Cu^+ complex[21]. However, complexes of Ni, Pd and Pt with L = 1,10-phenanthroline (phen) readily lose CO_2 upon collision-induced dissociation (Eq. 4). In the case of R = CH_3, the resultant organometallic ion readily reacts with acetic acid to regenerate $[(L)M(O_2CR)]^+$ (Eq. 5), thereby closing a catalytic cycle for the protodecarboxylation of acetic acid (Eq. 6) [22,23].

$$[(L)M(O_2CR)]^+ \rightarrow CO_2 + [(L)M(R)]^+ \quad (4)$$

$$[(L)M(CH_3)]^+ + CH_3CO_2H \rightarrow [(L)M(O_2CCH_3)]^+ + CH_4 \quad (5)$$

$$CH_3CO_2H \rightarrow CO_2 + CH_4 \quad (6)$$

In recent work, we showed that Pd(II) hydroccinnamate complexes with L = bis(diphenylphosphino)methane (dppm) undergo ligand-induced decarbonylation (Eq. 7), and the resulting organometallic product ion can lose styrene upon another stage of collisional activation (Eq. 8)[24].

$$[(L)Pd(O_2CCH_2CH_2C_6H_5)]^+ \rightarrow CO + [(LO)Pd(CH_2CH_2C_6H_5)]^+ \quad (7)$$

$$[(LO)Pd(CH_2CH_2C_6H_5)]^+ \rightarrow [(LO)Pd(H)]^+ + C_6H_5CH{=}CH_2 \quad (8)$$

Here we probe the efficiency of $[(L)M(O_2CR)]^+$ complexes with Ni(II) and Pd(II) and L = phen in catalyzing deoxygenation/fragmentation of fatty acids.

Results and Discussion

Fatty Acid Deoxygenation and Cracking

Previous studies have shown that nickel, palladium, and platinum can be efficiently utilized as heterogeneous catalysts for the deoxygenation and cracking of fatty acids[9]. The efficiency and length of hydrocarbons produced varies from metal to metal and its percentage in the catalyst[13]. Since thermodynamically, deoxygenation via decarboxylation (Eq. 1) is favorable (ΔG = -84 kJ/mol)[9] for stearic acid, experimental conditions needed to produce hydrocarbons are often not very harsh (300°C)[25].

Studying the deoxygenation reactions of the fatty acids in the gas phase allows us to gain insight into the mechanism and key intermediates involved. The first question is if this chemistry can be observed in carboxylate complexes (Eq. 4) where R is a long-chain fatty acid.

Indeed, cation complexes of the form $[(phen)M^{II}(O_2CR)]^+$ are easily formed through ESI for both Ni and Pd and, once collisionally activated in the ion trap, lose CO_2 (Figure 1 for R = $C_{17}H_{35}$, or stearic acid). Interestingly, in addition to decarboxylation, there are losses of H_2 and neutral hydrocarbons (C_nH_m). These neutral losses are consistently seen for saturated fatty acids independent of length (where R > C_2) with varying levels of abundance depending on fatty acid and identity of the metal. The data for other fatty acid complexes $[(phen)M^{II}(O_2CR)]^+$ are given in the SI (Figure S1, where R = *n*-C_3H_7 and *n*-C_9H_{19}).

For both nickel and palladium stearate complexes (Figure 1), loss of oxygen through decarboxylation is accompanied by varying levels of dehydrogenation. The difference in the pathway for deoxygenation is whether the deoxygenation is paired with dehydrogenation or not. In figure 1a, the deoxygenation of the nickel stearate complex occurs with dehydrogenation, with the main loss channel being -46 (CO_2 and H_2). The peaks associated with neutral loss of hydrocarbons smaller in length than the initial R, referred to in this work as the "cracking peaks", have extra steps of dehydrogenation that accompany them, leaving less saturated organometallic complexes. The deoxygenation and subsequent cracking of stearate-nickel species can be summarized with the following equations:

$$[(phen)M(O_2CC_{17}H_{35})]^+ \rightarrow [(phen)M(C_{16}H_{33-2x})]^+ + CO_2 + xH_2 \quad (9)$$
$$[(phen)M(C_{16}H_{33-2x})]^+ \rightarrow [(phen)M(C_{16-m}H_{33-2x-2m})]^+ + C_mH_{2m} \quad (10)$$

where $x \leq 3$.

The deoxygenation and cracking of the palladium species is similar to those of nickel, but in Pd case, x can also equal zero

which reflects the solo deoxygenation step that is observed, albeit as a very small fraction of combined deoxygenation/dehydrogenation (Fig. 1B, *m/z* 525, corresponding to the loss of 44 Da is about 1% of *m/z* 523, corresponding to the loss of 46 Da).

Cracking peaks observed for both nickel and palladium complexes corresponding to neutral losses of C_mH_{2m} can be further activated (through MS^n) to continue inducing "cracking" until the complex reaches either $[(phen)M(H)]^+$ or $[(phen)M(CH_3)]^+$

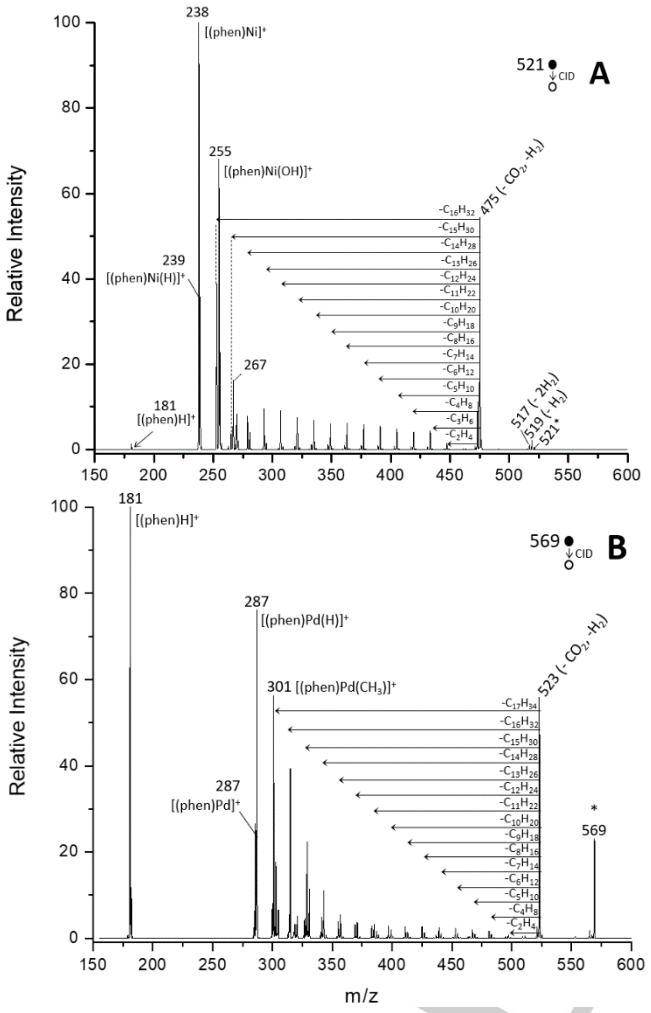

Figure 1. MS/MS of $[(phen)M(OOCC_{17}H_{35})]^+$ where M=Ni (a) and Pd (b). (*) indicates the precursor ion.

(Eqs 11 and 12). The mechanisms of these reactions are likely to involve a complex combination of "chain-walking" alkyl isomerization reactions[26,27]. The latter are the reverse of alkene insertion reactions of relevance to metal-catalyzed polymerization reactions, which have been extensively modelled via DFT calculations by Ziegler for Pd-based diimine polymerization catalysts[28–30].

$$[(phen)M(C_nH_m)]^+ \rightarrow [(phen)M(CH_3)]^+ + C_{n-1}H_{m-3} \quad (11)$$
$$[(phen)M(C_nH_m)]^+ \rightarrow [(phen)M(H)]^+ + C_nH_{m-1} \quad (12)$$

A prominent peak that can be seen in Figure 1A at *m/z* 255 corresponds to $[(phen)Ni(OH)]^+$. It is produced by reaction of residual water in the ion trap that can react with both product ions as shown in Eqs. 13 and 14 via the following reactions (data in figure S14):

$$[(phen)M(CH_3)]^+ + H_2O \rightarrow [(phen)M(OH)]^+ + CH_4 \quad (13)$$
$$[(phen)M(H)]^+ + H_2O \rightarrow [(phen)M(OH)]^+ + H_2 \quad (14)$$

A comparison of the length of hydrocarbon produced from gas-phase cracking can be compared between nickel and palladium and across the different fatty acids used, as shown for the stearate complexes in Figure 2.

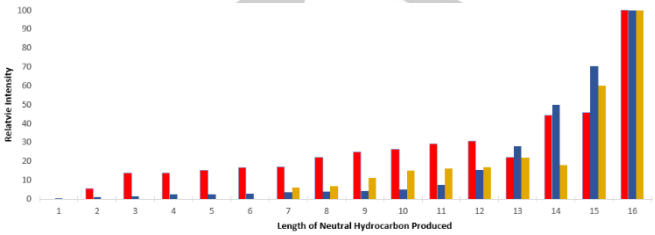

Figure 2. Comparison for neutral length of hydrocarbon lost after deoxygenation and cracking for stearate complexes. Our nickel (red) and palladium (blue) catalysts can be compared with Crocker's nickel catalyst (gold) from previously published work on cracking and deoxygenation of fatty acids and triglycerides[13]

For both Ni (red bars in Fig. 2) and Pd (blue bars) stearate complexes, the main product is C_{16} hydrocarbons resulting from deoxygenation with no cracking. This is consistent with the results of Crocker *et al.* on the deoxygenation and cracking of tristearin by a Ni/C catalyst, who showed that almost half of the products formed were resulting from deoxygenation alone with no cracking[13] (gold bars in Fig. 2). For $[(phen)Ni(OOCC_{17}H_{35})]^+$, formation of shorter chain hydrocarbons ($<C_{12}$) is favored, whereas for the palladium complex, higher amounts of long hydrocarbons are produced (C_{12}-C_{15}). The length of the hydrocarbons produced in the study by Crocker *et al.* was analyzed via GC and shows similar distribution of hydrocarbons (gold bars in Fig. 2) to what we observed in our gas-phase experiments[13].

Most of the previous gas-phase decarboxylation reactions (Eq. 4) were limited to simple coordinated anions such as formate, acetate, and benzoate[31,32] which undergo decarboxylation upon CID. Decarboxylation accompanied by dehydrogenation, as seen with the fatty acids above, can only be observed for carboxylic acids with α and β hydrogen atoms in the side chain. The simplest example of such a coordinated carboxylate is that derived from propionic acid ($C_2H_5CO_2H$). Thus, we chose propionic acid as a model for detailed studies, both experimental and computational, to investigate the mechanism and intermediates involved in fatty acid and carboxylic acid deoxygenation and dehydrogenation.

Propionic Acid as a Model for Deoxygenation

The CID spectra of the coordinated propionate cations, $[(phen)M(O_2CC_2H_5)]^+$, **1-M**, are shown in Figure 3A (M = Ni) and Figure 3B (M = Pd). In both cases peaks arising from deoxygenation of the coordinated propionate, **1-M**, are observed via the two competing pathways shown in Scheme 1 and give rise to $[(phen)M(C_2H_5)]^+$, **2-M** (via Eq. 4) and $[(phen)M(C_2H_3)]^+$, **3-M** (via Eq. 9). These channels correspond to the neutral losses of 44 (CO_2) and 46 [C,H_2,O_2], as confirmed via high-resolution mass spectrometry experiments (data in SI Table S1). In addition, prominent peaks due the formation of the hydrides, $[(phen)M(H)]^+$, **4-M**, are observed together with the products of their reaction with

water, which in the case of M = Ni gives rise to the hydroxide, $[(phen)Ni(OH)]^+$ (via Eq. 14), or the adduct $[(phen)Pd(H)(OH_2)]^+$. We cannot distinguish experimentally whether the hydrides are formed via stepwise fragmentation reactions (decarboxylation (Eq. 4) followed by β-hydride transfer (Eq. 12)) or in a single step (Eq. 15). This alternative, concerted mechanism, has been proposed to occur via a McLafferty-like rearrangement reaction proceeding though a six-centered TS for the gas-phase fragmentation of $[Cl_2Ca(O_2CR)]^-$ ions where R = C_2H_5 (propionate) or a larger chain[33].

$$[(phen)M(O_2CC_2H_5)]^+ \rightarrow [(phen)M(H)]^+ + CO_2 + C_2H_4 \quad (15)$$

For cations derived from acids, a loss of 46 Da is often attributed to decarbonylation with dehydration (loss of CO and H_2O)[34,35]. However since the neutral products of CID reactions are not detected and characterized in our experiments, we reviewed the available thermodynamic data on different neutral(s) of formula $[C,H_2,O_2]$ and performed DFT calculations. The NIST database of thermodynamic data[36] allowed us to evaluate the likelihood of several reasonable losses of 46 Da: i) CO + H_2O; ii) CO_2 and H_2: and iii) HCO_2H. These processes are all endothermic by 146, 105, and 121 kJ/mol but suggest that the loss of CO_2 and H_2 is the most likely scenario, at least, thermodynamically. The DFT calculations agree with the NIST data and are given in Scheme S1.

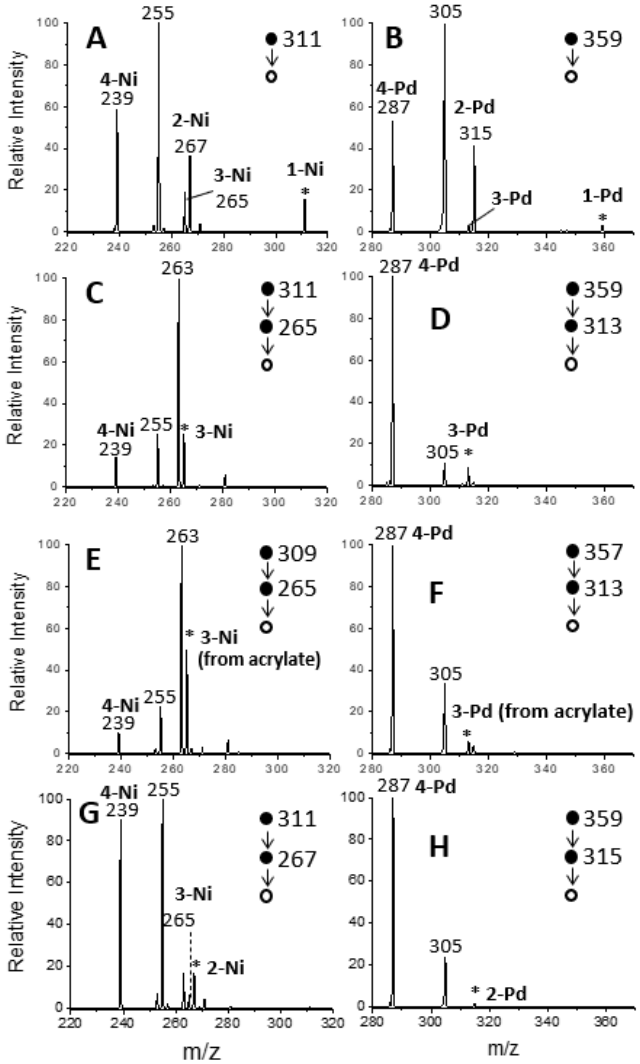

Figure 3. A) CID of $[(phen)Ni(O_2CC_2H_5)]^+$, **1-Ni** B) CID of $[(phen)Pd(O_2CC_2H_5)]^+$, **1-Pd** C) MS^3 of $[(phen)Ni(C_2H_3)]^+$, **3-Ni,** generated from propionic acid D) MS^3 of $[(phen)Pd(C_2H_3)]^+$, **3-Pd**, generated from propionic acid E) MS^3 of $[(phen)Ni(C_2H_3)]^+$, **3-Ni**, generated from acrylic acid authentic standard F) MS^3 of $[(phen)Pd(C_2H_3)]^+$, **3-Pd**, generated from authentic acrylic acid standard G) MS^3 of $[(phen)Ni(C_2H_5)]^+$, **2-Ni** H) MS^3 of $[(phen)Pd(C_2H_5)]^+$, **2-Pd**.

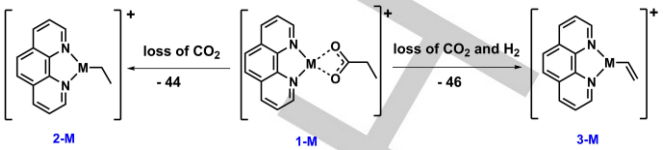

Scheme 1. Deoxygenation pathways for propionic acid.

In addition, both the NIST data and our DFT results show that decarboxylation alone (loss of 44 Da) is the most favorable pathway for deoxygenation of propionic acid by a large margin, being *exothermic* by ca. -29.3 kJ/mol[36], consistent with our DFT calculations (Scheme S1). Similarly, the thermodynamics of deoxygenation of stearic acid was reported by Crocker *et al.* with ΔG = -84 kJ/mol and -14 kJ/mol for decarboxylation and decarbonylation/dehydration, respectively[9].

Loss of 44 Da ***1-M → 2-M***		Pd	Ni
CO_2 loss	ΔH	39.4	100.8
	ΔE	49.5	111.1
	ΔG	-2.67	58.2
Loss of 46 Da ***1-M → 3-M***		Pd	Ni
$CO_2 + H_2$ loss	ΔH	211.5	259.9
	ΔE	252.5	300.1
	ΔG	131.7	180.2
CO + H_2O loss	ΔH	289.0	337.4
	ΔE	316.8	364.5
	ΔG	196.6	245.0
HCO_2H loss	ΔH	235.2	283.6
	ΔE	251.7	299.5
	ΔG	184.0	232.5

Table 1. Thermochemistry of fragmentation of **1-M** via Scheme 1.
[a]Enthalpies, energies, and free energies in kJ/mol, calculated at the B3LYP-D3BJ/BS2//M06/BS1 level of theory.

The corresponding thermodynamic data for the loss of 44 and 46 Da from the ionic species **1-M** was also calculated by DFT. The results are similar to the neutral propionic acid – decarboxylation is the least energy-demanding pathway (ΔE = 111.1 and 49.5 kJ/mol for **1-Ni** and **1-Pd**, respectively), while for the loss of 46 Da, the loss of CO_2 and H_2 is the least endothermic among the three possibilities calculated. The full compilation of the DFT-computed thermodynamics of deoxygenation of **1-M** species can be found in Table 1.

Most structures of species **1-M** – **3-M** (Scheme 1) were optimized computationally and can be found in the SI (Figure S2-S4). The loss of 46 from $[(phen)Ni(O_2CC_2H_5)]^+$ results in formation of $[(phen)Ni(C_2H_3)]^+$ which has only one reasonable structure corresponding to a metal-coordinated vinyl group. Experimental confirmation that the structure of species **3-M** has a coordinated vinyl anion was achieved by obtaining identical CID spectra from: i) $[(phen)Ni(C_2H_3)]^+$ formed via decarboxylation/dehydrogenation of $[(phen)Ni(O_2CC_2H_5)]^+$ (Figure 3C); and ii) an authentic standard formed by decarboxylation of the coordinated acrylate, $[(phen)Ni(O_2CCH=CH_2)]^+$ (Figure 3E).

Discussion of Mechanism for Loss of CO_2 and Other Fragmentation Reactions

We investigated the mechanism of decarboxylation of **1-M** computationally. Under the low-energy CID conditions used, the ions undergo multiple collisions with the helium bath gas resulting

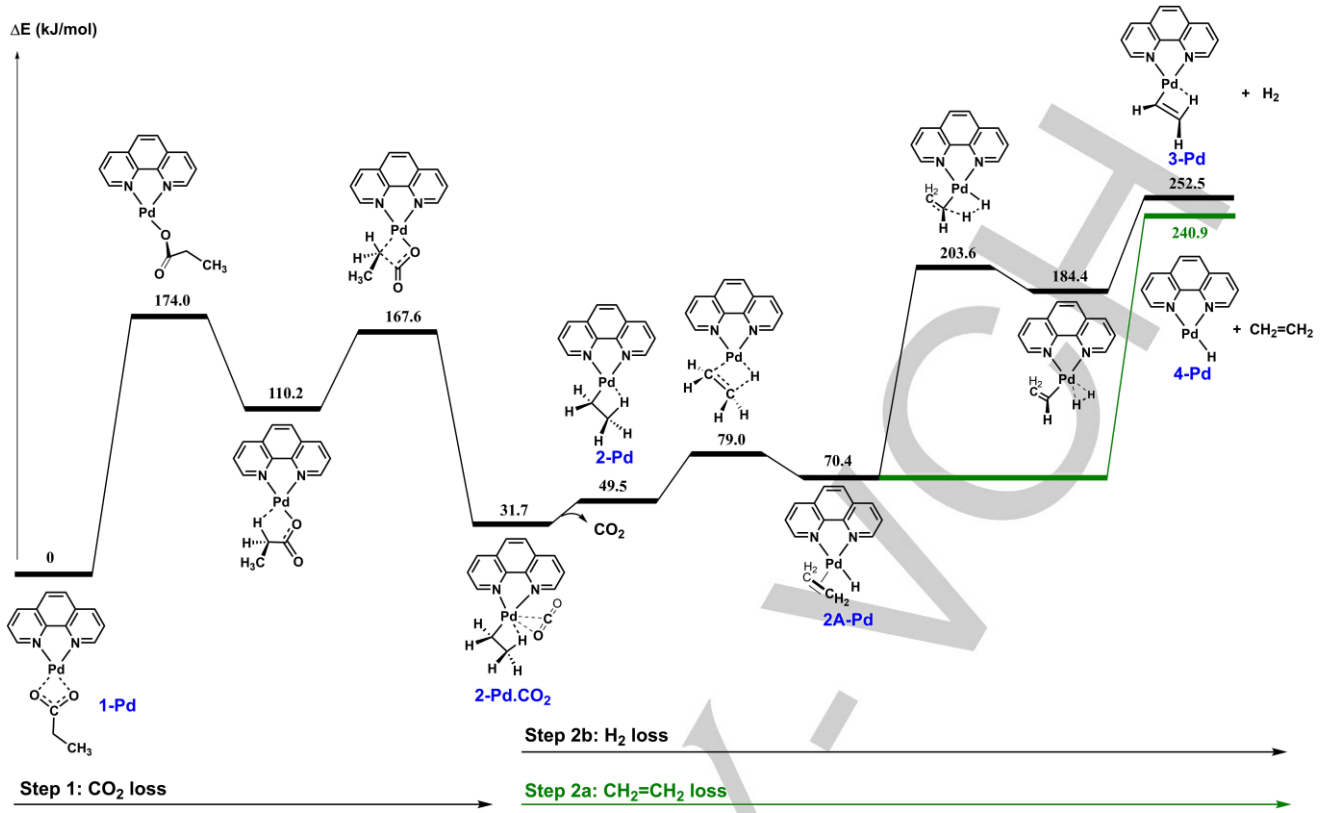

Figure 4: DFT calculated potential energy diagram for the decarboxylation of $[(phen)Pd(O_2CC_2H_5)]^+$, **1-Pd** followed by the competing fragmentation reactions of complex $[(phen)Pd(C_2H_5)]^+$, **2-Pd** proceeding via either □-hydride transfer to give $[(phen)Pd(H)]^+$, **4-Pd** or dehydrogentation to give $[(phen)Pd(C_2H_3)]^+$, **3-Pd**. The relative energies are given in kJ/mol and calculated at the B3LYP-D3BJ/BS2//M06/BS1 level of theory.

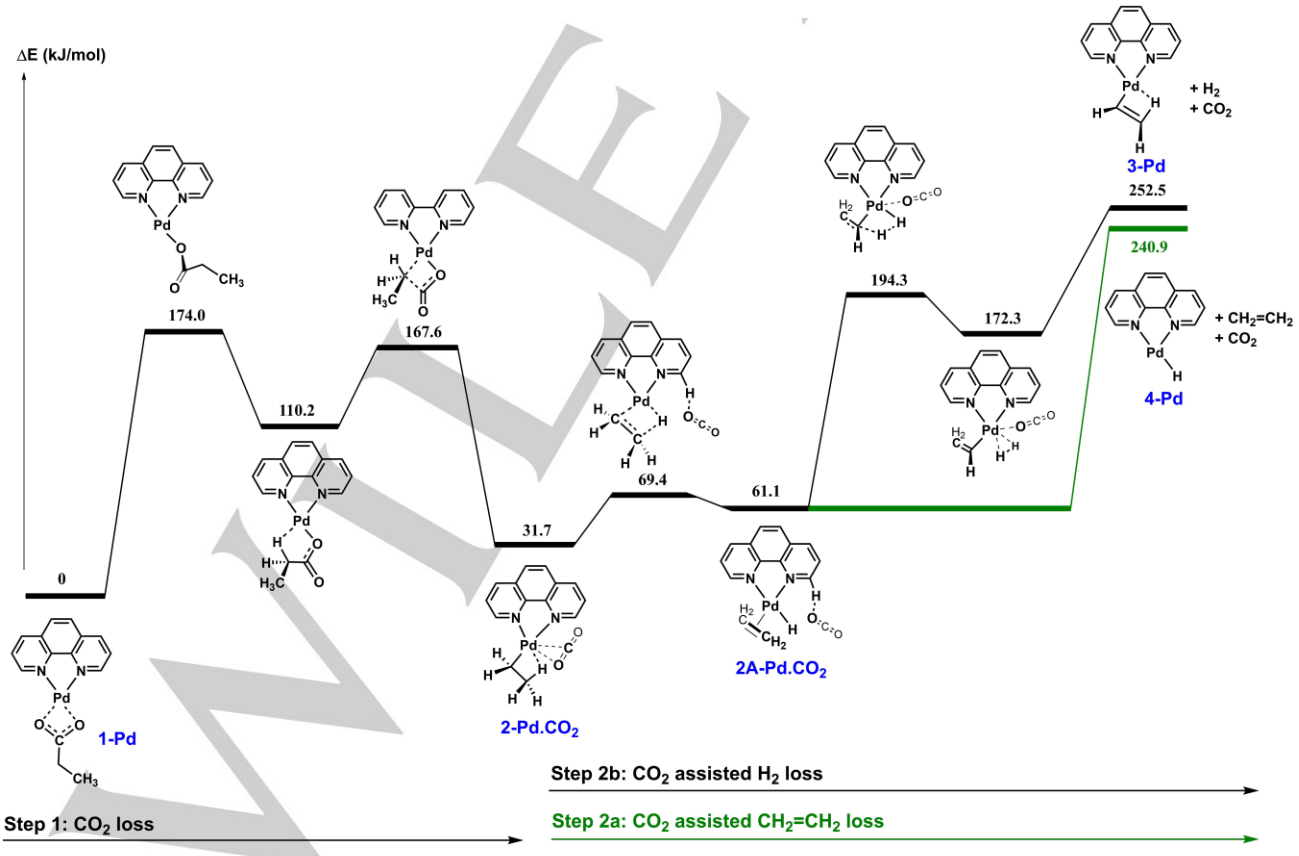

Figure 5. DFT calculated potential energy diagram for the sequential decarboxylation of $[(phen)Pd(O_2CC_2H_5)]^+$, **1-Pd** followed by the competing fragmentation reactions of CO_2 "solvated" complex $[(phen)Pd(C_2H_5)(CO_2)]^+$, **2-Pd.CO₂** proceeding via either β-hydride transfer to give $[(phen)Pd(H)]^+$, **4-Pd** or dehydrogentation to give $[(phen)Pd(C_2H_3)]^+$, **3-Pd**. The relative energies are given in kJ/mol and calculated at the B3LYP-D3BJ/BS2//M06/BS1 level of theory.

in an unknown temperature, herein we report on the ΔE of these reactions. The energy diagram for the loss of CO_2 from **1-Pd** is shown in Figure 4. The critical transition state (TS) at 174.0 kJ/mol is predicted to occur in the first step corresponding to the breakage of one of the carboxylate oxygen bonds to the metal. The magnitude of this barrier is easily achieved in typical ion trap CID experiments. The resulting conformer of **1-Pd** is then stabilized via agostic interactions between Pd and β-H atom of the side chain. Such interactions are quite well known[31,38], and their importance in subsequent fragmentation reactions will be addressed below. The next barrier, lower in energy than the critical one by 6.4 kJ/mol, corresponds to the extrusion of CO_2 via a four-membered TS, leading to the formation of organopalladium species **2-Pd**. The corresponding pathway for the decarboxylation of **1-Ni** is shown in Figure S5. The critical TS for Ni is calculated to be just a little higher than for Pd, at 189.5 kJ/mol.

In addition to the loss of CO_2, the CID spectra of **1-M** contain substantial amounts of $[(phen)M(H)]^+$, **4-M**, for both Ni and Pd (Figure 3A and 3B, respectively). They can be formed by sequential fragmentation of organometallic species **2-M** via eq. 15 ,concerted loss of CO_2 and C_2H_4. In order to directly compare the energy requirements for the sequential versus concerted losses, they are plotted from the same starting carboxylate complexes **1-M**. For these sequential reactions there are two scenarios: (1) fragmentation occurs via the bare **2-M**, which is shown as step 2a in Figure 4 for M = Pd; (2) the CO_2 remains "solvated" to **2-M** and the subsequent intermediates and transition states, thereby assisting these sequential reactions. For **1-Pd** the energy diagrams that allow direct comparison between the two stepwise and concerted reactions are shown as in Figure 4 (scenario (1)), Figure 5 (scenario (2)) and Figure 6 (McLafferty-like rearrangement).

An examination of Figure 4 reveals the most stable conformer of **2-Pd** displays substantial agostic interactions between Pd and the β-H atom of the ethyl moiety. The mechanism involves strengthening this Pd-H bond, which in turn leads to weakening of the Pd-C bond, until the intermediate becomes a complex of palladium hydride (**4-Pd**) with ethylene, similar to what has been described in literature[38]. This complex can either dissociate into **4-Pd** and C_2H_4 (via eq. 12), which is shown as step 2a, or undergo dehydrogenation via step 2b in which the hydride attacks an ethylene hydrogen to give the vinyl-H_2 complex, $[(phen)Pd(C_2H_3)(H_2)]^+$, which then fragment via release of H_2 to give $[(phen)Pd(C_2H_3)]^+$, **3-Pd**. Energetically, these two channels are very close to one another (within 9 kJ/mol) and should be experimentally competitive. However, fragmentation of **2-Pd** only produces **4-Pd** (loss of C_2H_4, Fig. 3H). Solvation by CO_2 (Figure 5) lowers the barrier for step 2b, and thus the observation of a minor amount of **3-Pd** may be due to this pathway.

The McLafferty-like rearrangement reaction for the concerted loss of CO_2 and C_2H_4 has its critical six-centered TS being about 261 kJ/mol above the reactants (Figure 6), significantly higher than both the first transition state associated with the decarboxylation step as well as the separated products. This suggests that the presence of **4-Pd** ions (*m/z* 287) in the CID spectrum of **2-Pd** is likely due to a stepwise process. Given that the barriers for stepwise CO_2 and H_2 loss lie below the separated

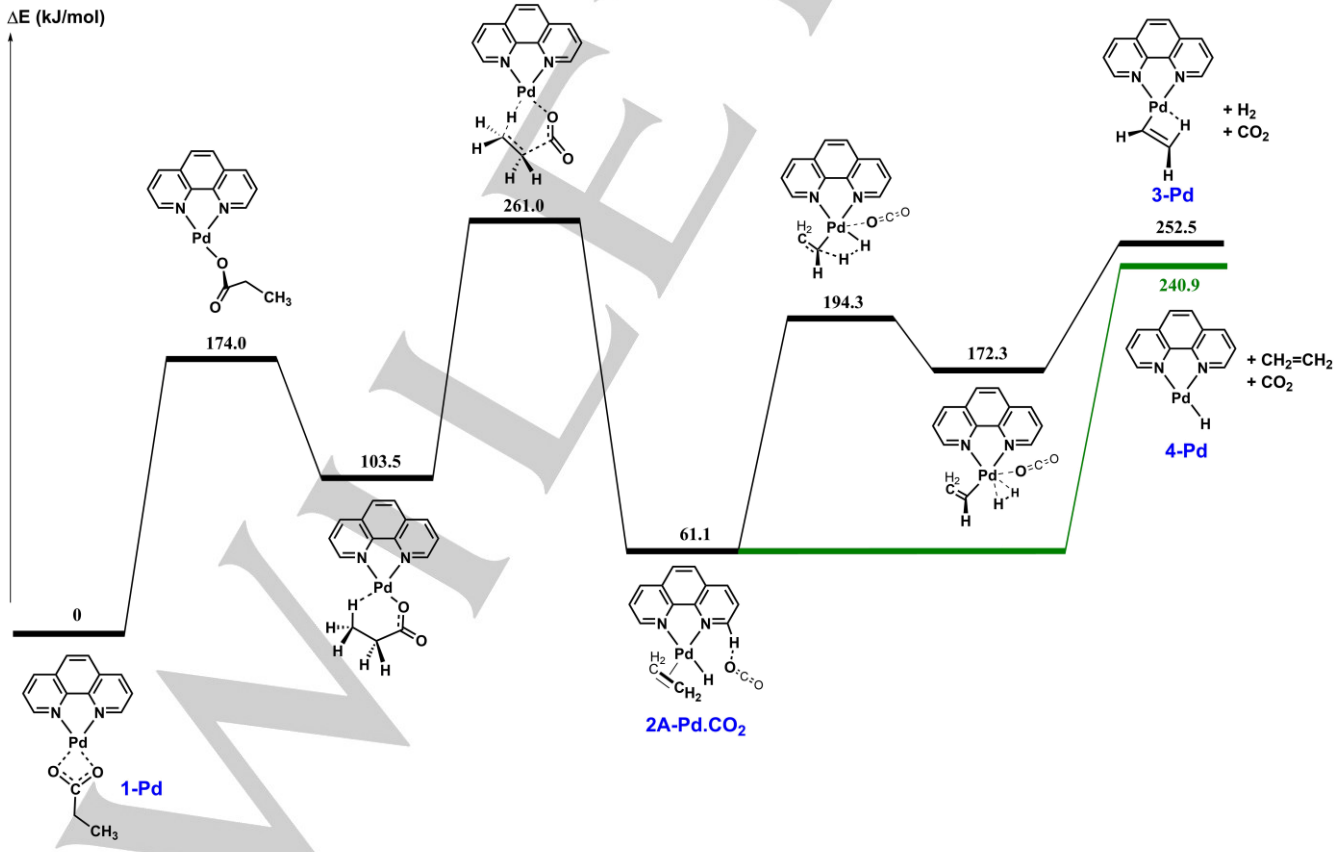

Figure 6. DFT calculated potential energy diagram for the concerted loss of CO_2 and C_2H_4 from $[(phen)Pd(O_2CC_2H_5)]^+$, **1-Pd**. The relative energies are given in kJ/mol and calculated at the B3LYP-D3BJ/BS2//M06/BS1 level of theory.

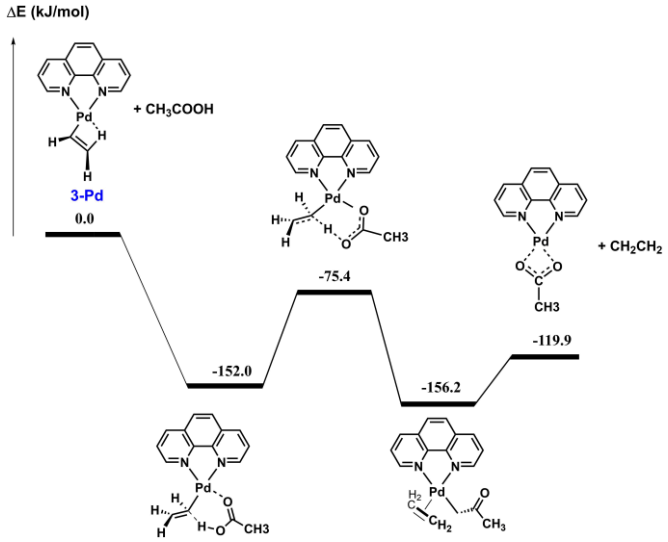

Figure 7. Energy diagram for the ion-molecule reaction between $[(phen)PdC_2H_3)]^+$, **3-Pd** and acetic acid, forming $[(phen)\mathbf{Pd}(OOC_2H_3)]^+$ and releasing CH_2CH_2. The relative energies are given in kJ/mol and calculated at the B3LYP-D3BJ/BS2//M06/BS1 level of theory.

products and even lower that the alternative separated prducts of H_2O and CO or HCO_2H, we have not probed these alternative pathways. Attempts to completely map out alternative reaction channels that involve H_2 loss to give a coordinated acrylate which then loses CO_2 were abandoned since the initial intermediates associated with C-H bond activation were high in energy (data not shown).

Finally, the corresponding energy profiles for the scenario 1, scenario 2 and McLafferty-like rearrangements of **1-Ni** are shown in Figure S5, S6 and S7. In the case of **2-Ni**, both channels are present, although loss of C_2H_4 still dominates.

Catalytic Cycle Involving Propionic Acid

As noted previously, ternary metal acetate complexes undergo decarboxylation via CID (eq. 4) and the resultant organometallic cation can then react with acetic acid to release methane and reform the initial acetate complex (eq. 5), thus closing the catalytic cycle of conversion of acetic acid into methane and carbon dioxide (eq. 6). [22,23] It is important to confirm whether similar cycles can operate for larger carboxylic acids. Continuing with propionic acid as the model, CID of the nickel propionate species, **1-Ni**, produces **2-Ni** via equation 4 and **3-Ni** via decarboxylation accompanied by H_2 loss (see Eq. 9), as shown in Figure 3A. Similar data for Pd are shown in Figure 3B.

Before tackling the reactivity of propionic acid, we investigated the reactivity of **2-M** and **3-M** towards acetic acid both experimentally and computationally. The $[(phen)M(C_2H_5)]^+$ ions (**2-Ni or 2-Pd**) did not react with acetic acid under our experimental conditions (data not shown). However, both **3-Ni** (Figure S8A) and **3-Pd** (data not shown) displayed reactivity towards acetic acid as shown in Eq. 16.

$$[(phen)M(C_2H_3)]^+ + CH_3CO_2H \rightarrow [(phen)M(O_2CCH_3)]^+ + C_2H_4 \quad (16)$$

In addition, species **4-M**, formed upon CID of **3-M** via Eq. 12 or directly from **1-M** via Eq. 15, readily reacted with acetic or propionic acid via Eq. 17 (mass spectra shown in Figure 8C and 8D for propionic acid; reaction of **4-Ni** with acetic acid is shown in Figure S8, data for **4-Pd**/acetic acid not shown). This is not surprising considering the fact that numerous metal hydride complex ions have been shown to react with carboxylic acids via acid-base hydrogen recombination[39,40].

$$[(phen)M(H)]^+ + CH_3CO_2H \rightarrow [(phen)M(O_2CCH_3)]^+ + H_2 \quad (17)$$

Under the low-pressure IMR conditions used, only the total energy of the separated reactants is available to fuel reactivity and so ΔE is used to provide a measure of whether a reaction is possible or not[41]. DFT calculations performed for the palladium species were consistent with our experimental findings. For example, the energy profile for the reaction of **3-Pd** with acetic acid (Eq. 16) shows an exothermic reaction (Figure 7). Once the ion **3-Pd** and acetic acid form an ion-molecule reactant complex, this transforms into the corresponding product complex via a transition state where the metal is bound to both vinyl and acetate. In the case of **3-Pd**, this TS energy is below that of separated reactants, thus, the ion-molecule reaction is observed.

Similar reaction energy profiles for **2-Pd, 2-Ni**, **3-Ni**, **4-Pd,** and **4-Ni** are shown in Figures S9 - S13 and the data are summarized in Table 2. As can be seen, DFT predicted that the behavior of **4-Pd** would be similar to that of **3-Pd**. However, no reaction would occur between **2-Pd** and acetic acid, since the TS for this reaction is located *higher in energy* than the separated reactants. This can be explained by the different extent of agostic interactions in **2-Pd** vs **3-Pd**. In **2-Pd**, the interactions between the metal and the β hydrogen atom of the CH_3 group are estimated to be ca. 54.2 kJ/mol (the energy difference between the lowest-energy conformer of **2-Pd** with agostic interactions and the one where the ethyl moiety is rotated away from the metal as shown in Figure S3).Such strong agostic interactions were also found in ligated Ni(II)-ethyl complexes in solution and crystals[42]. In contrast, agostic interactions in **3-Pd** are much weaker (ca. 4.1 kJ/mol, Figure S4) as it is much harder for the metal to form a bond with the β hydrogen atom of the rigid vinyl moiety. This difference explains the lower reaction exothermicity and higher TS energy for **2-Pd** and thus higher reactivity of **3-Pd** towards acetic acid.

Table 2. Energetics of ion-molecule reactions with acetic acid.

Species	TS Energy[a] (barrier[b])	Reaction enthalpy
2-Pd	+7.2 (85.2)	-70.2
3-Pd	-75.4 (76.6)	-109.2
4-Pd	-54.4 (197.0)	-104.7

Energies in kJ/mol

[a]Relative to separated reactants

[b]Relative to the reactant ion-molecular complex

Similar reactions can be carried out with propionic acid as shown in Figure 8. The corresponding catalytic cycles are shown in Scheme 2. Both cycles display the overall reaction (Eq. 18).

$$C_2H_5CO_2H \rightarrow C_2H_4 + H_2 + CO_2 \quad (18)$$

Catalytic deoxygenation and hydrocarbon production from larger fatty acids

Some of the findings for the propionic acid model system can now be applied to the longer-chain fatty acids, such as stearic

acids. Revisiting Figure 1, it can be seen that fragmentation of $[(phen)M(O_2CC_{17}H_{35})]^+$ results in very little decarboxylation (loss

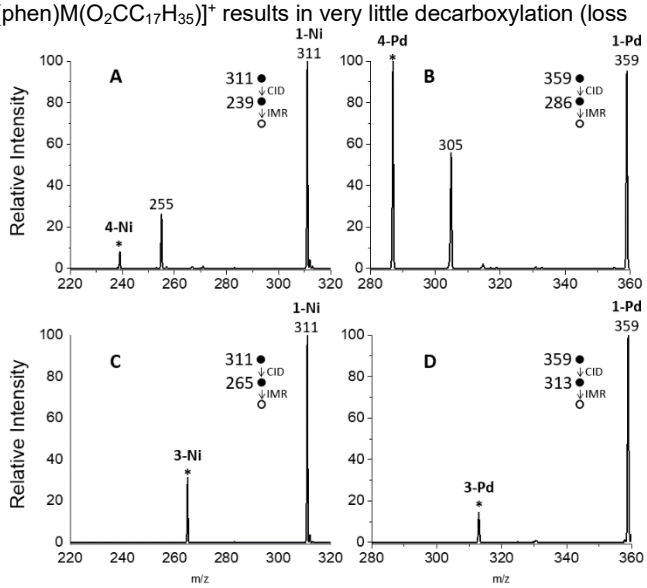

Figure 8. Ion-molecule reactions of **4-M** (A and B) and **3-M** (C and D) with propionic acid.

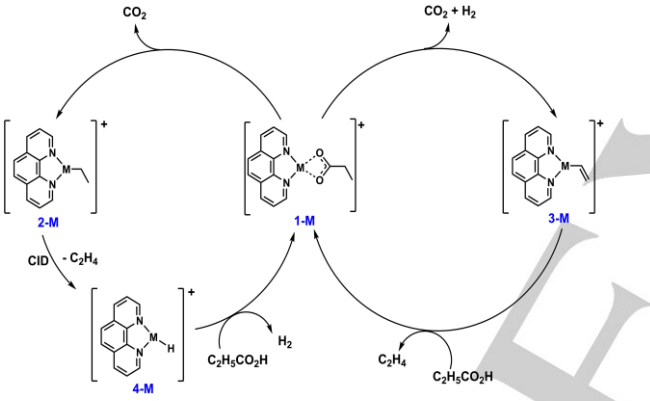

Scheme 2. Catalytic cycles for deoxygenation of propionic acid.

of CO_2 only) but mostly proceeds with a combined loss of CO_2 and H_2 via Eq. 9, similar to the pathway described in Figures 4-5. The pathway of eliminating the whole alkene from the chain ($C_{17}H_{34}$) via Eq. 12, shown for the model system in the same Figure 5, is also prominent, as spectra for both M=Ni and M=Pd show prominent **4-M** peaks at *m/z* 239 and 287, respectively. It seems that in larger systems the barriers for these processes are lower relative to that for the loss of CO_2.

The main difference between fragmentation of stearate and propionate complexes is the series of "cracking" peaks shown in Figure 1 formally corresponding to the loss of alkenes from C_2H_4 to $C_{16}H_{32}$ from the $[(phen)M(C_{17}H_{33})]^+$ intermediate, which, in turn, is generated via Eq. 9. Thus, alkenes must be extruded from the organometallic species via a "chain-walking"-type mechanism common for Ni(II) and Pd(II) catalysts used for alkene polymerization/depolymerization[24,41]. Detailed investigation of this mechanism in such gas-phase systems is being published in a separate study. The processes described in this work can be catalyzed by Ni, Pd (and Pt), whilst other first-row transition metal ions (Co, shown in figure S15 and Cu, shown in figure S16) did not induce deoxygenation and cracking of fatty acids under the similar conditions.

We should also point out that the deoxygenation/cracking catalyzed by Ni and Pd complexes proceeds via a very different mechanism from the well-known charge-remote fragmentation of fatty acid/alkali (or alkaline earth) metal ion complexes[43]. While the charge-remote fragmentation also results in the extrusion of alkenes from the fatty acid chain[44], it originates from the opposite side of the chain (from the end opposite to the carboxylate moiety), does not result in decarboxylation, and does not operate via catalytic cycle described here.

To "close the catalytic cycle", these fragment ions need to be converted to the precursor carboxylate species, $[(phen)M(O_2CR)]^+$. Thus, we studied the reactivity of every fragment ion towards acetic acid. Similar to the behavior of **2-M** ions ($[(phen)M(C_2H_5)]^+$), longer-chain complexes of the general formula $[(phen)M(C_nH_m)]^+$, where n>2, exhibit a lack of reactivity towards acetic acid. This can be rationalized by the strong agostic interactions that would occur with the longer, more flexible hydrocarbon chain, in line with the discussion above for **2-M**. However, like with the propionic acid model, upon further steps of MS^n, fatty acid cracking product ions eventually yield shorter-chain species (**3-M**, Eq. 10; **4-M,** Eq. 12 and $[(phen)M(CH_3)]^+$, Eq. 11). Reactions of **3-M** and **4-M** with acetic and propionic acids proceeded readily and were discussed above.

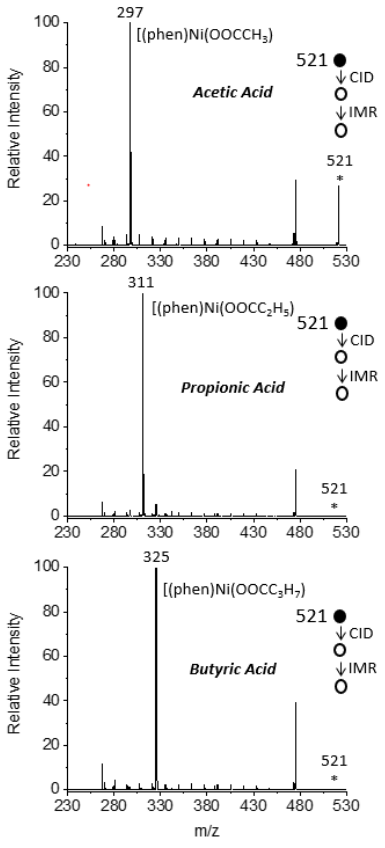

Figure 9. Ion-molecule reaction of ions produced from CID of $[(phen)Ni(OOCC_{17}H_{35})]^+$ with acetic acid (a) propionic acid (b) and butyric acid (c).

Species $[(phen)M(CH_3)]^+$ were shown previously to react with acetic acid via Eq. 5, and the mechanism for this reaction was computationally studied in detail for M = Ni, Pd, and Pt.[22,23]

In order to complete the catalytic cycle similar to the one shown in Scheme 2 using longer-chain acids such as stearic acid,

a neutral stearic acid would need to be introduced into the ion trap. Unfortunately, due to the low volatility of these acids, this is not feasible. However, reactions with propionic and butyric acids were studied and the resulting spectra are displayed in Figure 9.

Here, the mixture of cracking fragments formed by CID from $[(phen)Ni(OOCC_{17}H_{35})]^+$ (shown in Figure 1A) are subjected to a reaction with the neutral acids. The fragment ions of the general formula $[(phen)M(C_nH_m)]^+$, where n>2, did not react, but the higher-intensity ions seen in Figure 1A all reacted completely with the neutral carboxylic acids. The hydride (**4-Ni**) at *m/z* 239 reacted by releasing H_2 via eq. 17; the methyl complex $[(phen)M(CH_3)]^+$ at *m/z* 253 produced CH_4 (eq. 5); and the vinyl complex (**3-Ni**) at *m/z* 265 reacted by releasing C_2H_4 via eq. 16. All these reactions also resulted in the formation of the carboxylate complex ions, $[(phen)Ni(O_2CR)]^+$, (R = CH_3, C_2H_5, or C_3H_7), which represented the base peaks in each of the spectra in Figure 9 (individual spectra for the reactions with acetic acid given in figure S8). This strongly suggests that under the appropriate conditions, catalytic cycles similar to those in Scheme 2 would operate for stearic acid as well.

Conclusion

The ternary Ni(II) and Pd(II) complexes $[(phen)M(O_2CR)]^+$ (where phen = 1,10-phenanthroline; R = C_nH_{2n+1}, n≥2) can be easily formed in solution and transferred into the gas phase through electrospray ionization. Unlike the ternary complexes of carboxylic acids with simple side chains (formic, acetic, benzoic) that undergo decarboxylation upon CID, these complexes with longer side chains show more complex fragmentation chemistry. In addition to decarboxylation, their CID also results in deoxygenation via loss of $[C,H_2,O_2]$, that according to DFT calculations is most likely the combined loss of CO_2 and H_2. The CID spectrum of the stearate complexes (R = $C_{17}H_{35}$) also shows a series of cations $[(phen)M(R')]^+$ (where R' < C_{17}) separated by 14 Da (CH_2) corresponding to losses C_2H_4 - $C_{16}H_{32}$ which are referred to as "cracking products". Detailed experimental and theoretical studies of the molecular model – the propionate complex, $[(phen)M(O_2CC_2H_5)]^+$ - were conducted and shed a light on the potential mechanisms of decarboxylation and subsequent loss of H_2 or the side-chain-alkene C_2H_4.

Multiple stages of CID of the cracking products $[(phen)M(R')]^+$ eventually lead to $[(phen)M(H)]^+$ and $[(phen)M(CH_3)]^+$. Both of these ions react with volatile carboxylic acids, RCO_2H, (acetic, propionic, and butyric) to reform carboxylate complexes $[(phen)M(O_2CR)]^+$. This shows that the ternary Ni and Pd complexes serve as catalysts in fragmentation of the fatty acids. In contrast, cracking products with longer carbon chains, $[(phen)M(R)]^+$ (R > C_2), were found to be unreactive towards these carboxylic acids. This was consistent with DFT calculations that predicted strong agnostic interactions between the metal and β hydrogen atom of the hydrocarbon chain. These interactions increase the barrier for the ion-molecule reaction with the carboxylic acid.

Experimental Section

Materials: Palladium acetate, nickel acetate, acetic acid, propionic acid, butyric acid, and stearic acid were all purchased from Sigma-Aldrich (St. Louis, MO, USA) and used as received. Solutions were prepared by mixing equal volumes of ligand, metal, and fatty acid (1 mg/mL) in MeOH and diluting to 0.1 mg/mL in MeOH. Samples were allowed to react for five minutes to allow for the complexation of the metal, ligand, and fatty acid. Solutions were then introduced into the mass spectrometer via electrospray ionization.

Mass Spectrometry: Other than the high resolution experiments, all mass spectrometry experiments were carried out on a ThermoFisher LTQ (ThermoFisher Scientific, San Jose, CA, USA) with a modification to the helium line to allow for ion-molecule reactions; the modification is described in detail in other sources[45]. For the high resolution scans a Bruker Maxis II Qq-TOF was used. Samples were introduced into the instruments through electrospray ionization at a flow rate of 5 μL/min. Source parameters were set to 5 kV needle voltage, 275 °C inlet temperature, and 3 a.u. for nitrogen gas flow rate. Complex precursor ions of the form $[(L)M(O_2CR)]^+$ were isolated in the ion trap with a window of about 1 *m/z* and subjected to collision-induced dissociation at a normalized collision energy (NCE) between 20-22% ensuring maximum product intensity. For the ion-molecule reactions (IMR) in the LTQ, the neutral acetic, propionic, and butyric acids were all introduced as liquids into the helium line through the bypass at a flow rate of 0.01 μL/hr, allowing them to enter the ion trap and react with the trapped ions. The reaction time could be varied by adjusting the scan time delay of the instrument.

DFT Calculations: Gaussian09 was used[46] to fully optimize the structures as singlets at the M06 level of density functional theory (DFT)[47]. SDD basis set was chosen to describe Pd and Ni[48,49] while 6-311G(d) basis set was used for other atoms[50]. This basis set combination is referred to as BS1. Frequency calculations were carried out at the same level of theory as those for the structural optimization. Transition structures were located using the Berny algorithm. Intrinsic reaction coordinate (IRC) calculations were used to confirm the connectivity between transition structures and minima[51,52]. To further refine the energies obtained from the M06/BS1 calculations, single-point energy calculations were carried out for all the structures with the larger def2-TZVPP basis set (BS2) for all atoms[53] at the B3LYP-D3BJ level of theory[54–57]. The B3LYP-D3BJ calculations were used to account for long-range correlation for dispersion forces. To estimate the corresponding enthalpy, ΔH, and Gibbs energies, ΔG, at 298K the corrections were calculated at the M06/BS1 levels and finally added to the corresponding single-point energies. Single point corrected energies obtained from the B3LYP-D3BJ/BS2//M06/BS1 calculations are reported throughout unless otherwise stated.

Acknowledgements

We acknowledge the support of the ARC (DP180101187 funding to AJC and RAJO), and the National Computing Infrastructure. We also acknowledge the generous support from NSF MRI program (award # CHE:1726931 to VR) for the purchase of the high-resolution mass spectrometer.

Keywords

Biomass conversion; density functional theory calculation; gas-phase reactions; homogeneous catalysis; Mass spectrometry

[1] P. McKendry, *Rev. Issue* **2002**, *83*, 37–46.
[2] P. McKendry, *Rev. Issue* **2002**, *83*, 47–54.
[3] P. McKendry, *Rev. Issue* **2002**, *83*, 55–63.
[4] P. Weiland, *Eng. Life Sci.* **2006**, *6*, 302–309.
[5] M. Mohammad, T. Kandaramath Hari, Z. Yaakob, Y. Chandra Sharma, K. Sopian, *Renew. Sustain. Energy Rev.* **2013**, *22*, 121–132.
[6] V. L. Dagle, C. Smith, M. Flake, K. O. Albrecht, M. J. Gray, K. K. Ramasamy, R. A. Dagle, *Green Chem.* **2016**, *18*, 1880–1891.

[7] T. Morgan, E. Santillan-Jimenez, A. E. Harman-Ware, Y. Ji, D. Grubb, M. Crocker, *Chem. Eng. J.* **2012**, *189–190*, 346–355.
[8] L. Rantanen, R. Linnaila, P. Aakko, T. Harju, SAE International, **2005**.
[9] E. Santillan-Jimenez, M. Crocker, *J. Chem. Technol. Biotechnol.* **2012**, *87*, 1041–1050.
[10] E. Santillan-Jimenez, T. Morgan, J. Lacny, S. Mohapatra, M. Crocker, *Fuel* **2013**, *103*, 1010–1017.
[11] J. M. Clark, M. R. Nimlos, D. J. Robichaud, *J. Phys. Chem. A* **2014**, *118*, 260–274.
[12] P. Sabatier, *Catalysis in Organic Chemistry*, D. Van Nostrand Company, **1922**.
[13] T. Morgan, D. Grubb, E. Santillan-Jimenez, M. Crocker, *Top. Catal.* **2010**, *53*, 820–829.
[14] A. S. Berenblyum, V. Ya. Danyushevsky, E. A. Katsman, T. A. Podoplelova, V. R. Flid, *Pet. Chem.* **2010**, *50*, 305–311.
[15] D. Kubička, L. Kaluža, *Appl. Catal. Gen.* **2010**, *372*, 199–208.
[16] Q. Smejkal, L. Smejkalová, D. Kubička, *Chem. Eng. J.* **2009**, *146*, 155–160.
[17] X. Sun, J. Chen, T. Ritter, *Nat. Chem.* **2018**, *10*, 1229–1233.
[18] D. Schröder, W. Zummack, H. Schwarz, *J. Am. Chem. Soc.* **1994**, *116*, 5857–5864.
[19] T. Yalcin, J. Wang, D. Wen, A. G. Harrisoncor, *J. Am. Soc. Mass Spectrom.* **1997**, *8*, 749–755.
[20] C. L. Gatlin, F. Tureček, *J. Mass Spectrom.* **1995**, *30*, 1636–1637.
[21] C. L. Gatlin, F. Turecek, T. Valsar, *Anal Chem* **1994**, 3950–3958.
[22] M. Woolley, G. N. Khairallah, G. da Silva, P. S. Donnelly, R. A. J. O'Hair, *Organometallics* **2014**, *33*, 5185–5197.
[23] M. J. Woolley, G. N. Khairallah, G. da Silva, P. S. Donnelly, B. F. Yates, R. A. J. O'Hair, *Organometallics* **2013**, *32*, 6931–6944.
[24] M. Lesslie, Y. Yang, A. J. Canty, E. Piacentino, F. Berthias, P. Maitre, V. Ryzhov, R. A. J. O'Hair, *Chem. Commun.* **2018**, *54*, 346–349.
[25] M. Snåre, I. Kubičková, P. Mäki-Arvela, K. Eränen, D. Yu. Murzin, *Ind. Eng. Chem. Res.* **2006**, *45*, 5708–5715.
[26] L. Guo, S. Dai, X. Sui, C. Chen, *ACS Catal.* **2016**, *6*, 428–441.
[27] D. Janssen-Müller, B. Sahoo, S.-Z. Sun, R. Martin, *Isr. J. Chem.* **2019**, *0*, DOI 10.1002/ijch.201900072.
[28] A. Michalak, T. Ziegler, *Organometallics* **1999**, *18*, 3998–4004.
[29] A. Michalak, T. Ziegler, *Organometallics* **2000**, *19*, 1850–1858.
[30] A. Michalak, T. Ziegler, *J. Am. Chem. Soc.* **2002**, *124*, 7519–7528.
[31] E. L. Piacentino, E. Rodriguez, K. Parker, T. M. Gilbert, R. A. J. O'Hair, V. Ryzhov, *J. Mass Spectrom.* **2019**, *54*, 520–526.
[32] R. A. J. O'Hair, N. J. Rijs, *Acc. Chem. Res.* **2015**, *48*, 329–340.
[33] G. Rodríguez-Blanco, K. J. Jobst, T. M. Luider, J. K. Terlouw, P. C. Burgers, *ChemPlusChem* **2013**, *78*, 1184–1189.
[34] R. A. O'Hair, P. S. Broughton, M. L. Styles, B. T. Frink, C. M. Hadad, *J. Am. Soc. Mass Spectrom.* **2000**, *11*, 687–696.
[35] S. Xu, J. Pavlov, A. B. Attygalle, *J. Mass Spectrom.* **2017**, *52*, 230–238.
[36] S. G. Lias, J. E. Bartmess, J. Liebman, J. Holmes, R. D. Levin, *J. Phys. Chem. Ref. Data* **1988**, *17*, 1–861.
[37] S. A. McLuckey, D. E. Goeringer, *J. Mass Spectrom.* **1997**, *32*, 461–474.
[38] M. Brookhart, M. L. H. Green, G. Parkin, *Proc. Natl. Acad. Sci.* **2007**, *104*, 6908–6914.
[39] E. L. Piacentino, K. Parker, T. M. Gilbert, R. A. J. O'Hair, V. Ryzhov, *Chem. – Eur. J.* **2019**, *25*, 9959–9966.
[40] G. N. Khairallah, A. Richard, *Int. J. Mass Spectrom.* **2006**, *254*, 145–151.
[41] P. D. Dau, P. Armentrout, M. C. Michelini, J. K. Gibson, *Phys. Chem. Chem. Phys.* **2016**, *18*, 7334–7340.
[42] F. M. Conroy-Lewis, L. Mole, A. D. Redhouse, S. A. Litster, J. L. Spencer, *J. Chem. Soc. Chem. Commun.* **1991**, 1601–1603.
[43] C. E. Randolph, D. J. Foreman, S. K. Betancourt, S. J. Blanksby, S. A. McLuckey, *Anal. Chem.* **2018**, *90*, 12861–12869.
[44] M. Cordero, C. Wedemiotis, *Anal. Chem.* **1994**, 861–866.
[45] S. Gronert, *J. Am. Soc. Mass Spectrom.* **1998**, *9*, 845–848.
[46] M. Frisch, G. W. Trucks, H. B. Schlegel, G. E. Scuseria, M. A. Robb, J. R. Cheeseman, G. Scalmani, V. Barone, B. Mennucci, G. ea Petersson, others, **2014**.
[47] Y. Zhao, D. G. Truhlar, *Theor. Chem. Acc.* **2008**, *120*, 215–241.
[48] M. Dolg, U. Wedig, H. Stoll, H. Preuss, *J. Chem. Phys.* **1987**, *86*, 866–872.
[49] D. Andrae, U. Haeussermann, M. Dolg, H. Stoll, H. Preuss, *Theor. Chim. Acta* **1990**, *77*, 123–141.
[50] A. McLean, G. Chandler, *J. Chem. Phys.* **1980**, *72*, 5639–5648.
[51] K. Fukui, *J. Phys. Chem.* **1970**, *74*, 4161–4163.
[52] K. Fukui, *Acc. Chem. Res.* **1981**, *14*, 363–368.
[53] F. Weigend, R. Ahlrichs, *Phys. Chem. Chem. Phys.* **2005**, *7*, 3297–3305.
[54] A. D. Becke, *Phys. Rev. A* **1988**, *38*, 3098.
[55] C. Lee, W. Yang, R. G. Parr, *Phys. Rev. B* **1988**, *37*, 785.
[56] P. J. Stephens, F. Devlin, C. Chabalowski, M. J. Frisch, *J. Phys. Chem.* **1994**, *98*, 11623–11627.
[57] A. D. Becke, *J. Chem. Phys.* **1993**, *98*, 5648–5652.

TABLE OF CONTENTS

Fatty acid deoxygenation/cracking in the gas phase: Fatty acids can be catalytically deoxygenated and "cracked" to produce a mixture of hydrocarbons via complexing with Ni^{2+} or Pd^{2+} and 1,10-phenanthroline inside a mass spectrometer. The detailed deoxygenation mechanism is described for propionic acid as a model system.

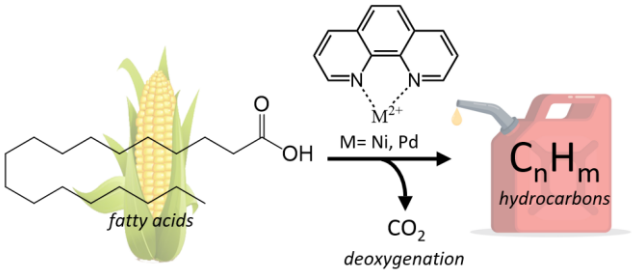

Kevin Parker, Dr. Geethika Weragoda, Victoria Pho, Prof. Allan J. Canty, Prof. Anastasios Polyzos, Prof. Richard A. J. O'Hair, Prof. Victor Ryzhov

Page No. – Page No.

Gas-Phase Models for the Nickel- and Palladium-Catalyzed Deoxygenation of Fatty Acids